Modeling and Analysis of Normal Stress in Viscoelastic Dampers

M. R. Eskafi*
Department of Mechanical and Aerospace Engineering
Science and Research Branch Islamic Azad University, Tehran, Iran
Email:Mohamad.Eskafi@gmail.com
*Corresponding author

N. Ashrafi & M. Najafi
Department of Mechanical and Aerospace Engineering
Science and Research Branch Islamic Azad University, Tehran, Iran
Email:n_ashrafi@hotmail.com, M.Njafi36@gmail.com

Received: 16 June 2011, Revised: 14February 2011, Accepted: 13 May 2012

Abstract: A custom-made nonlinear viscoelastic damper is designed for several industrial applications. The damper is structurally similar to typical commercial dampers and the design is solely based on the choice of the viscoelastic material used as damping agent in the damper. With rheological parameters of a selected material from experiment, the coefficients of Johnson-Segalman constitutive equation model are evaluated by fitting the data. The problem was first formulated by introducing the governing equations for the flow over flat plate. A numerical scheme of finite difference method is applied to solve the governing equations in the time domain. The model is capable of predicting the nonlinear amplitude-dependent behavior of viscoelastic dampers under single and multiple-frequency excitations.

Keywords: Johnson Segalman Model, Non-Newtonian Flow, Rheological Model, Stability Analysis, Viscoelastic Damper

Reference: Eskafi, M. R., Ashrafi, N. and Najafi, M., "Modeling and Analysis of Normal Stress in Viscoelastic Dampers", Int J of Advanced Design and Manufacturing Technology, Vol. 6/ No. 1, 2013, pp. 49-59.

Biographical notes: M.R. Eskafi has received his MSc in Mechanical Engineering at the Islamic Azad University, Tehran, Iran. He is interested in viscoelastic materials. **N. Ashrafi** holds a PhD in Mechanical Engineering from University of Western Ontario in Canada. His research interests include non-Newtonianfluid dynamics, stability, and rheology. He has so far published more than 20 papers in international journals as well as several conference proceedings. He has held several positions in research and industry, e.g., postdoctoral fellowship at the University of Wales (UK), researcher at Shell Research Center (UK), faculty member at Georgia Southern University (USA), University of Natal(South Africa) and Islamic Azad University (Iran). **M. Najafi** received his PhD in Mechanical Engineering from the University of Alabama in 1989. His current research interests include energy storage systems, cooling systems, heating systems, meshless numerical works in heat transfer and fluid flow in thermodynamic analysis.

1 INTRODUCTION

In order to enhance the application of the damping agent in industrial dampers, we have introduced elasticity in the fluid. The influence of fluid elasticity is therefore examined for the plane Couette flow (PCF) of a Johnson-Segalman (JS) fluid. Similar to shear thinning, fluid elasticity is an inherent property of polymeric fluids used in materials processing, which cannot be ignored. While the presence of inertia alone can destabilize the flow, fluid elasticity or normal stresses give rise to additional nonlinearities and coupling among the flow variables, making an already complex problem even more difficult to solve.

Similar to any flow in the transition regime, the PCF of viscoelastic fluids involves a continuous range of excited spatiotemporal scales. In order to assess the effect of the motion of the arbitrarily many smaller length and time scales, one would have to resolve in detail the motion of the small scales. This issue remains unresolved since, despite the great advances in storage and speed of modern computers, it will not be possible to resolve all continuous ranges of scales in the transition regime.

It is by now well established that low-order dynamical systems can be a viable alternative to conventional numerical methods as one strives to probe the nonlinear range of flow behavior [1], [2]. The relative simplicity of low-order dynamical systems, and the rich sequence of nonlinear flow phenomena exhibited by their solution, have been the major contributing factors to their widespread use as models for examining the onset of chaotic motion. Despite the severe degree of truncation in the formulation of these equations, some of the basic qualitative elements is recovered using a low-order dynamical model.

Since the seminal work of Lorenz [3], low-order dynamical systems have typically been used to handle simple flow configurations [4], particularly the Rayleigh-Benard thermal convection [5-7] and Taylor-Couette flow problems. The validity of the low-dimensional description was also established. For example, in the Taylor-Couette flow of a Newtonian fluid, the solution to the full Navier-Stoke equations was obtained by implementing a finite-difference scheme, and an approximate approach based on the Galerkin representation. Comparison of flows based on the two methods led to good agreement.

In the Galerkin approximation, the velocity and stress components assume truncated by Fourier or other orthogonal representations in space, depending on the boundary conditions, and the expansion coefficients are functions of time alone, thus leading to a nonlinear system up projection of the equations onto the various modes. The stability of PCF is examined by adopting a low-order nonlinear dynamical system approach and the Galerkin projection method. More recently, attempts have been made to apply low-order dynamical systems for complex geometry particularly focused on the instability of PCF of high-molecular-weight fluids, typically composed of a Newtonian solvent and a polymeric solute.

Although low-order dynamical systems have mainly been formulated for Newtonian fluids, they have only recently been attempted for non-Newtonian flows. Khayat and associates implemented a low-order dynamical system approach for non-Newtonian fluids in thermal convection of rotating flows [8].

In particular, purely shear thinning flows were modeled using truncation levels similar to the Lorenz model. In this case nonlinearities stem from inertia and the dependence of viscosity on the rate-of-strain tensor, but the resulting three-dimensional system is similar to the Lorenz equations.

It must be noted that this level of truncation is too severe to expect any meaningful physics far beyond the critical point to be captured. However, low-order models can be useful in giving a simplified version of the complex dynamics that is bound to arise when higher-order modes are included. This is what has been observed in the case of purely elastic fluid systems. Low levels of truncation were used for the flow of viscoelastic fluids with constant viscosity, obeying the Oldroyd-B constitutive model.

In this case, the nonlinearities stem from inertia and the upper-convected terms in the constitutive equation. Despite the severe level of truncation, results based on low-order dynamical system approach have been encouraging; as good conformity was obtained between experimental results, and theoretical results concluded from linear stability analysis and conventional formulations whenever possible, especially for the Teylor-Couette flow. The earlier study focused on the interplay between inertia and elasticity.

While the problem of stability of PCF has been extensively investigated for Newtonian fluid, relatively little attention has been devoted to the flow of viscoelastic fluids. The presence of viscoelasticity is expected to dramatically alter the stability picture in PCF. This is mainly due to the presence of additional nonlinearities that are usually part of any realistic constitutive model.

What adds to the controversy is the fact that theoretical studies on channel (Couette and Poiseuille) flow using the more popular constitutive models, such as Maxwell and Oldroyd-B fluids, were found to be linearly stable. More recently, linear stability analysis based on the JS model showed that the base channel flow can become unstable for a range of Weissenberg number coinciding with the negative slope of the steady-state stress/shear curve. Recently, seismic analysis of structures with

viscoelastic dampers modeled by the Kelvin chain and the Maxwell ladder is presented in ref. [9].
The present paper explores the critical and nonlinear range of instability of PCF of a JS fluid, where conventional method, such as the finite-element method would have difficulty in yielding a solution. The formulation is based on a truncated expansion of the velocity and stress in terms of orthogonal functions. At the two critical Weissenberg numbers, which coincide with the two extrema of the shear-stress/shear-rate curve, there is an exchange of stability that occurs between the linear Couette flow and other nonlinear steady-state flows.

2 PROBLEM FORMULATION

The dynamical system for a JS fluid for the PCF is derived in this section to an arbitrary level of approximation. The low-order model, with six degrees of freedom, is obtained as a special case. The general equations for a viscoelastic fluid are first discussed. Finally, the coherence of the model is addressed to ensure the reliability of the proposed method.

2.1. Governing equation for one-dimensional channel flow

Consider the flow of an incompressible viscoelastic fluid of density 'ρ', relaxation time 'λ', and viscosity 'η', between two infinite flat plates separated by a distance 'd'. The upper and lower plates are assumed to move at constant velocity $U_B/2$in opposite directions. In this study, only fluids that can be reasonably represented by a single relaxation time and constant viscosity are considered. The fluid considered here is a polymer solution composed of a Newtonian solvent and a polymer solute of viscosities 'η_s' and 'η_p', respectively; therefore$\eta = \eta_s + \eta_p$. In general, the flow is governed by the continuity and conservation of momentum equations for an incompressible fluid, which, in dimensional form, are given by Eqs. (1a) and (1b).

$$\nabla . U = 0 \quad (1a)$$

$$\rho(U_t + U.\nabla U) = -\nabla P + \nabla . T + \eta_s \nabla^2 U \quad (1b)$$

Where 'U' is the velocity vector, 'P' is the pressure, 'T' is the polymeric contribution of the stress tensor, 'τ' is the time, and '∇'is the gradient operator. A comma denotes partial differentiation. The constitutive equation adopted in this study corresponds to the JS model as given by Eq. (1c) [10].

$$\lambda \frac{DT}{Dt} + T = \eta_P [\nabla U + (\nabla U)^t] \quad (1c)$$

where $(\nabla U)^t$ denotes the transpose of ∇U , and we use Eqs. (2), (3) and (4) for definition of $\frac{DT}{Dt}$.

$$\frac{DT}{Dt} = \left(1 - \frac{\zeta}{2}\right) T^{\nabla} + \frac{\zeta}{2} T^{\Delta} \quad (2)$$

$$T^{\nabla} \equiv T_{,t} + U.\nabla T - (\nabla U)^t.T - T.\nabla U \quad (3)$$

$$T^{\Delta} \equiv T_{,t} + U.\nabla T + T.(\nabla U)^t + \nabla U.T \quad (4)$$

Equations (5), and (6) define both lower and upper convective terms. Here $\zeta \in [0,2]$, which is a dimensionless material (slip) parameter.
The value of 'ζ'is a measure of the contribution of no affine motion to the stress tensor. For $\zeta = 0$, the motion is affine and the Oldroyd-B model is recovered, whereas for $\zeta = 2$, the motion is completely nonaffine and the model is reduced to the Oldroyd–Jaumann model. When $\zeta = 0$and $\eta_s = 0$, the upper-convected Maxwell model is recovered.
In this study the PCF is examined in the(X, Y)plane, where the X axis lies halfway and along the two plates. Only one-dimensional$(1\text{-}D)$disturbances in the X direction are examined. In this case, if U denotes the axial velocity along X (with V, the velocity component along the Y direction, being zero), then the nondimensional variables can be introduced by Eq. (5).

$$u = \frac{U\lambda}{d}, t = \frac{T}{\lambda}, y = \frac{Y}{d}, p = \frac{P\lambda}{\eta_p}, \tau_{ij} = \frac{T_{ij}\lambda}{\eta_p} \quad (5)$$

where $i, j = X, Y$. Therefore, Eq. (1) led to Eq. (6).

$$Re\, u_{,t} = \epsilon u_{,yy} + \tau_{xy,y} \quad (6a)$$

$$\tau_{xx,t} = -\tau_{xx} + (2 - \zeta) u_{,y} \tau_{xy} \quad (6b)$$

$$\tau_{yy,t} = -\tau_{yy} - \zeta u_{,y} \tau_{xy} \quad (6c)$$

$$\tau_{xy,t} = -\tau_{xy} + u_{,y} - \frac{\zeta}{2} u_{,y} \tau_{xx} + \left(1 - \frac{\zeta}{2}\right) u_{,y} \tau_{yy} \quad (6d)$$

Stick boundary conditions are assumed to hold at the two plates and we have Eq. (7).

$$u(y = \pm\tfrac{1}{2}, t) = \pm\frac{We}{2} \quad (7)$$

where the Reynolds number, Re, the Weissenberg number,We, and the solvent-to solute viscosity ratio, ϵ,

are the three similarity groups of the problem, which are given, respectively, by Eq. (8).

$$Re = \frac{d^2\rho}{\eta_p \lambda}, We = \frac{U_B \lambda}{d}, \boldsymbol{\epsilon} = \frac{\eta_s}{\eta_p} \quad (8)$$

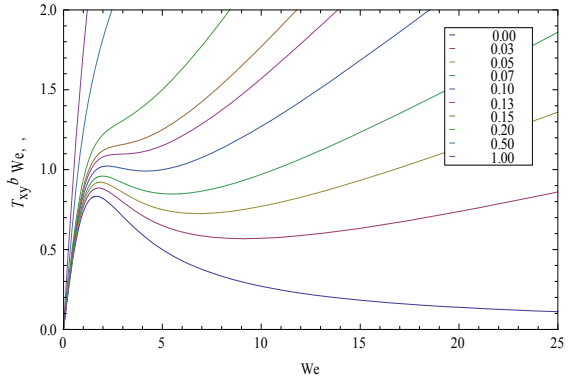

Fig. 1 Steady-State shear stress/shear-rate curves in the (T_{xy}^b, We) plane for $\zeta = 0.2$ $(a = -0.18)$, AND $\epsilon \in [0,1]$

The base (Couette) flow corresponding to the steady-state solution of Eq. (6) is given by Eq. (9).

$$u^b = We\, y \quad (9a)$$

$$\tau_{xy}^b = \frac{We}{1+\zeta(2-\zeta)We^2} \quad (9b)$$

$$\tau_{xx}^b = \frac{(2-\zeta)We^2}{1+\zeta(2-\zeta)We^2} \quad (9c)$$

$$\tau_{yy}^b = -\frac{\zeta We^2}{1+\zeta(2-\zeta)We^2} \quad (9d)$$

The total steady shear stress T_{xy}^b in this case may be written as

$$T_{xy}^b = \boldsymbol{\epsilon}\, We + \frac{We}{1+\zeta(2-\zeta)We^2} \quad (9e)$$

Equation (9d) is probably the most revealing result of the JS model. It reflects the possibility of a nonmonotonic behavior for the stress/shear-rate relation. Indeed, Fig. 1 shows the behavior of the shear stress, T_{xy}^b, as a function of We for $\boldsymbol{\epsilon} \in [0,1]$ and $\zeta = 0.2$. Fig. 1 indicates that the stress curves tend to have two extrema (a maximum and a minimum), which tend to merge as $\boldsymbol{\epsilon}$ increases.

This situation is a reminiscent of the load/deformation behavior in elasticity. In the case of nonlinear inflation of Mooney–Rivlin (hyperelastic) membranes, for instance, the pressure also exhibits a similar behavior as a function of the stretch ratio for various Mooneyconstants. Upon comparing the curves in Fig. 1, the case of an Oldroyd-B fluid $(\xi = 0)$is comparable to the caseof a neo-Hookean solid, while the curve for a Newtonianfluid$(\epsilon = 1)$is comparable to the curve of a Hookean solid.

There are two additional curves included in Fig. 1, namely those corresponding to the two extrema. These curves are important because, as it turns outand will be seen in the following, they correspond to the critical Weissenberg numbers between which the base flowloses its stability. Equation (6) is further simplified if cast in terms of the normal stress difference,N, and a combination of normalstresses, Z, such that is presented in Eq. (10).

$$N = \tau_{xx} - \tau_{yy},\ Z = \frac{\zeta}{2}\tau_{xx} + \left(1 - \frac{\zeta}{2}\right)\tau_{yy} \quad (10)$$

However, Z is found to decay exponentially with time andexhibits uninteresting transient behavior. It will thus be setequal zero.It is convenient to seek the departure in velocityu'andstress$\tau'_{ij}$from the base flow, which are introduced by Eq. (11) as follows.

$$u = u^b + u',\ \tau_{ij} = \tau_{ij}^b + \tau'_{ij} \quad (11)$$

The flow departure is hence governed by Eq. (12) as follows.

$$Re\, u_{,t} = \epsilon u_{,yy} + S_{,y} \quad (12a)$$

$$N_{,t} = -N + 2\left(We\, S + S u_{,y} + S^b u_{,y}\right) \quad (12b)$$

$$S_{,t} = -S + u_{,y} + a\left(We\, N + N u_{,y} + N^b u_{,y}\right) \quad (12c)$$

Where the prime is dropped in Eq. (10) and the following abbreviations are introduced by Eq. (13).

$$S^b = \tau_{xy}^b,\ N^b = \tau_{xx}^b - \tau_{yy}^b,\ a = \zeta\left(\frac{\zeta}{2} - 1\right) \quad (13)$$

Note that the departure shear stress is given by $S = \tau_{xy}$. Note also that the flow departure, u, N, and S have zero value at thetwo plates. It is interesting to observe from Eq. (12) that the inclusion of inertia does not alter the steady-state solution.

2.2. Galerkin projection and the dynamical system

The solution of Eq. (12) is carried out using the Galerkin projection method. The variables$u\,(y,t), N(y,t)$, and $S(y,t)$are represented by series of Chandrasekhar functions that satisfy the homogeneous (no-slip) boundary conditions. Asuitable level of truncation is imposed, which leads to the final nonlinear dynamical system. A judicious selection process is applied for the choice of various modes in order toensure the physical and mathematical

coherence of the final model. The general series representations for the velocityand normal stress difference are given by Eq. (14).

$$u(y,t) = \sum_{i=1}^{M} u_i(t)\phi_i(y) \quad (14a)$$

$$N(y,t) = \sum_{i=1}^{M} N_i(t)\phi_i(y) \quad (14b)$$

Whereas the shear stress representation is taken as:

$$S(y,t) = \sum_{i=1}^{M} S_i(t)\phi_i'(y) \quad (14c)$$

Where$\phi_i(y)$ are the even and odd Chandrasekhar functions, for i even and odd, respectively [11],and$\phi_i'(y)$are defined as$\phi_i'(y) = (1/\alpha_i)(d\phi_i/dy)$, where $\alpha_i$are constants. Here M is the number of modes.The first step in the Galerkin projection method consists of substituting expressions (14) into Eq. (12). Each of the equations in (12) is then multiplied by the appropriate mode and is integrated over $y \in [-1/2, 1/2]$. Thus a set of nonlinear and coupled ordinary differential equations which govern the time-dependent expansion coefficients is obtained. The projection leads to explicit expressions for the time derivative of u_k and $N_k, k \in [1, M]$ and Eq. (15) is introduced as follows,

$$\frac{du_k}{dt} = \frac{1}{Re}\sum_{i=1}^{M} \alpha_i(\epsilon\alpha_i u_i + S_i)A_{ik} \quad (15a)$$

$$\frac{dN_k}{dt} = -N_k + 2\sum_{i=1}^{M}\left[(WeS_i + S^b\alpha_i u_i)B_{ik} + \sum_{j=1}^{M}\alpha_i u_i S_j C_{ijk}\right] \quad (15b)$$

The stress coefficients, S_k, are governed implicitly by

$$\sum_{i=1}^{M}\left\{\left[\frac{dS_i}{dt} + S_i - (1 + aN^b)\alpha_i u_i\right]D_{ik} - a\,WeB_{ki}N_i - a\alpha_i u_i\sum_{j=1}^{M} N_j C_{ikj}\right\} = 0 \quad (15c)$$

Where $A_{ik} = \langle\phi_i''|\phi_k\rangle$, $B_{ik} = \langle\phi_i'|\phi_k\rangle$, and $C_{ijk} = \langle\phi_i'\phi_j'|\phi_k\rangle$ are constants defined through the integral operation$\langle .|. \rangle \equiv \int_{-1/2}^{1/2} .. dy$.

The derivatives(dS_k/dt)can beobtained explicitly in terms of the expansion coefficients either analytically or numerically depending on the number of modes used. The solution of Eq. (15) is obtained after a suitable truncation level is introduced. From now on it will be referred to as system (B1).

2.3. Coherence of the low-order model

To any level of truncation, it should be ensured that the truncation has not caused a singularity in the low-order model resulting from Eq. (15), and that the model remains physically coherent, similarly to the original Eq. (12). The discussion is limited to system (B1). To this end, a Lyapunov function is introduced for the model and it is shown that the solution of system (B1) remains bounded.

In other words, we must show that the (phase) velocity field in $\Re^6$ from every other direction is directed towards the origin on a surface surrounding the origin, and is located at a large distance from it. Let $F(u_1, u_2, N_1, N_2, S_1, S_2) = 0$ be the equation for such a surface. Thus, one must have Eq. (16), everywhere in phase space.

$$DF = \dot{u}_1 F_{,u_1} + \dot{u}_2 F_{,u_2} + \dot{N}_1 F_{,N_1} + \dot{N}_2 F_{,N_2} + \dot{S}_1 F_{,S_1} + \dot{S}_2 F_{,S_2} < 0 \quad (16)$$

There is a wide range of possibilities for the choice of the surface F. Consider Eq. (17), (six-dimensional) ellipsoid among all the possibilities as follows.

$$F = \frac{1}{2}(A_1 u_1^2 + A_2 u_2^2 + B_1 N_1^2 + B_2 N_2^2 + D_1 S_1^2 + D_2 S_2^2) - \infty \quad (17)$$

Where $A_1, A_2, B_1, B_2, D_1, D_2$ are arbitrary and positiveconstants to be specified, and '∞' is positive and arbitrarily large. Upon substituting Eq. (17) into Eq. (16), using system (B1), and requiring the coefficients of dominant cubic terms to vanish, it is found that B_1, B_2, D_1 and D_2 must be zero, leading to Eq. (18).

$$DF = \frac{\epsilon}{Re}(C_1 A_1\alpha^2 + C_2 A_2\beta^2), F = \frac{1}{2}(A_1 u_1^2 + A_2 u_2^2) - \infty \quad (18)$$

Since C_1 and C_2 are negative, it is clear that DF remains negative, and it can be concluded that, inthis case, no trajectory originating from a point with a finitedistance from the origin can go off to infinity.Consider now the coherence of the model.

The issue is volume contraction in phase space. Similarly to the original Eq. (1), system (B1) must be dissipative. Thus, a volume, V(t),in phase space must contract with time. For volume contraction to be insured, the velocity field must have a constant negative divergence everywhere, leading to Eq. (19).

$$\frac{1}{V(t)}\frac{dV(t)}{dt} = \frac{\partial\dot{u}_1}{\partial u_1} + \frac{\partial\dot{u}_2}{\partial u_2} + \frac{\partial\dot{N}_1}{\partial N_1} + \frac{\partial\dot{N}_2}{\partial N_2} + \frac{\partial\dot{S}_1}{\partial S_1} + \frac{\partial\dot{S}_2}{\partial S_2} = \frac{\epsilon}{Re}(C_1\alpha^2 + C_2\beta^2) - 4 \quad (19)$$

Again, since C_1 and C_2 are both negative, VdV/dt willalwaysbe negative as well. Hence, if a set of initial points inphase space initially occupy a region $V(0)$, then after sometime t, the end points of the

corresponding trajectories willfill a volume, leading to Eq. (20).

$$V(t) = V(0)exp\left[\frac{\epsilon}{Re}(C_1\alpha^2 + C_2\beta^2) - 4\right]t \qquad (20)$$

Which indicates that the volume decreases exponentially with time. The above-mentioned analysis is restricted to the six dimensional system. Although a similar analysis can be carried out along the same lines of arguments, it is hardly envisage able how this can be done in practice when an arbitrary number of modes are involved.

The search for a Lyapunov function would be particularly difficult. Additional assessment of the coherence of the model will be made next when linear stability analysis is carried out. In this case, a comparison will be carried out between the exact and approximate solutions.

3 STABILITY ANALYSIS

In this section, linear stability of the base (Couette) flow is carried out first. The steady-state solutions of system (B1)are then obtained, and their stability, away from the critical points, is investigated through linear stability analysis. Then the stability near the critical points is addressed.

3.1. Stability of the Couette flow

Consider a small departure from the base flow given by Eq. (9). Upon linearizing system (B1) around the base flow, two sets of decoupled cubic characteristic equations are obtained. These equations exhibit the same dependence on Re, We, ζ, and ϵ. Each of these equations, governing the eigen-value Λ, may be compactly written for reference in the form of Eq. (21).

$$Re\Lambda^3 + A(Re, We, \zeta, \epsilon)\Lambda^2 + B(Re, We, \zeta, \epsilon)\Lambda + C(We, \zeta, \epsilon) = 0 \qquad (21)$$

Where $A, B,$ and C are complicated expressions that neednotbe given explicitly here. It is found that, for given $\boldsymbol{\epsilon}$ and ζ, the eigen-value Λ is generally real for small Re. In this case, the decay or growth of the flow near the base flow is monotonic.

The issue of monotonic versus oscillatory behavior will be addressed. For small We, Λ (or its real part) remains negative and decreases in amplitude as Weincreases.As We reaches a critical value We_{c1}, one of theroots (or its real part) changes sign. Another change in signal so occurs when We reaches a second critical value $We_{c2} > We_{c1}$.

There is thus an exchange of stability between the base flow and another (nontrivial) steady-state flow at $We = We_{c1}$. As will be seen below, there is a nontrivial steady-state branch for $We_{c1} < We < We_{c2}$. At $We = We_{c2}$, there is another exchange of stability, this time between the nontrivial branch and the base flow. That is, the base flow becomes stable again for $We > We_{c2}$.

The values of We_{c1} and We_{c2} can be found by monitoringthe sign of the real part of Λ, by varying We and keepingRe fixed. However, since the loss of stability of the base flowcoincides with the onset of the nontrivial branch, and sincethe steady-state solutions do not depend on Re, then the critical Weissenberg numbers should not depend on Re.

Thus,We_{c1} and We_{c2} can be found by examining only the characteristicequations corresponding to $Re = 0$, which, from Eq. (21), turn out to be quadratic and is of the form: $\Lambda^2 + D(We, \zeta, \epsilon)\Lambda + E(We, \zeta, \epsilon) = 0$. Moreover, D happens to be always positive so that We_{c1} and We_{c2} are obtained bysolving the equation $E = 0$. Thus, the two critical Weissenbergnumbers are given by Eq. (22).

$$We_{c1,c2} = \sqrt{\frac{\epsilon+(\epsilon-1)C_6C_8}{4a\epsilon C_6C_8} \pm \frac{1}{2}\sqrt{\left(\frac{(\epsilon-1)C_6C_8+\epsilon}{2a\epsilon C_6C_8}\right)^2 - \frac{1+\epsilon}{\epsilon a^2 C_6C_8}}} \qquad (22)$$

An important question should be addressed regarding the nature of the bifurcation at the critical points. In the most general case, this equation has one real root and two complex conjugate roots.

In general, for a Hopf bifurcation to emerge, the cubic characteristic equation must have two imaginary (conjugate) roots at $We = We_{c1}$or We_{c2}. By examining thecoefficients of the cubic equations, it is not difficult to establish that a Hopf bifurcation cannot emerge at the critical Weissenberg numbers. The process of parameter identification is an inverse problem which is over determined and can be ill conditioned [12].

When $Re = 0$, an analytical characteristic equation can beobtained directly for the original Eq. (6). The resulting marginal curves can be compared with the approximate curves based on Eq. (22), thus allowing the assessment of the validity of the approximate analysis and solution. The exact characteristic equation in this case turns out to be the quadratic Eq. (23) as follows.

$$\Lambda^2 + \left[2 + \frac{1}{\epsilon(1-2aWe^2)}\right]\Lambda + \left[\frac{1+2aWe^2+\epsilon(1-2aWe^2)^2}{\epsilon(1-2aWe^2)}\right] = 0 \qquad (23)$$

Equation (23) indicates that the real root of Λ vanishes when the third term on the left-hand side vanishes. Hence, the exact critical Weissenberg numbers can be readily obtained as Eq. (24).

$$We_{c1,c2} = \sqrt{\frac{1}{4a\epsilon}\left(2\epsilon - 1 \pm \sqrt{1-8\epsilon}\right)} \qquad (24)$$

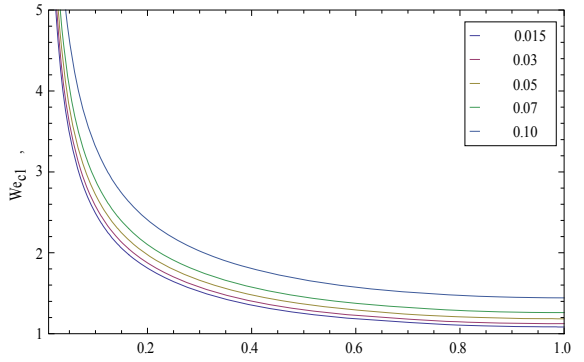

(a)

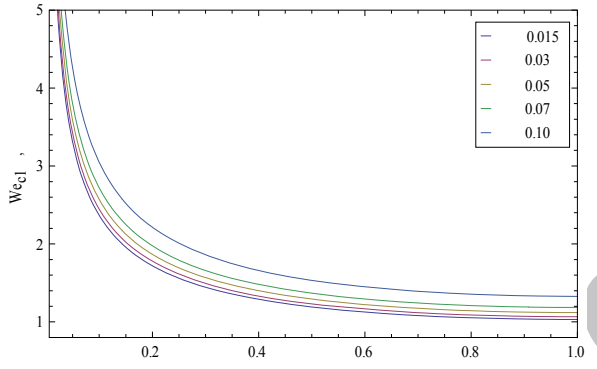

(b)

Fig. 2 Marginal stability curves for $\epsilon \in [0.015,0.10]$ for the first critical weisenberg number We_{C1}. The curves are plotted against ζ for the range [0,1]. Note that the curves are symmetric with respect to $\zeta = 1$. The approximate curves based on the six-dimensional model system (B1) are shown in (a), and the exact curves are shown in (b)

The equation also indicates that there is no possibility for a Hopf bifurcation at We_{c1} and We_{c2}. It is important to observethat the roots, We_{c1} and We_{c2}, given by Eq. (24)are the same as those at which the shear stress, τ_{xy}^{b}, reaches it maximum and minimum values, respectively. Note that they merge for $\epsilon = 1/8$(see also Fig. 1).

Thus, the base flow is unstable for the region lying between the two extremes of the curves in Fig. 1. For the applicable range of ϵ the relative difference between the critical Weissenberg numbers (22) and (24) is found to be less than 6%. This is a small discrepancy given the low number of modes used in the solution representation.

The agreement between the exact and approximate marginal stability curves is illustrated in Fig. 2 in the (We_{c1}, ζ) plane, and in Fig. 3 in the (We_{c2}, ζ) plane for$\epsilon \in [0.02,0.1]$. For the first critical Weissenberg number, Fig.2(a) shows the approximate curves and Fig. 2(b) shows the exact curves.

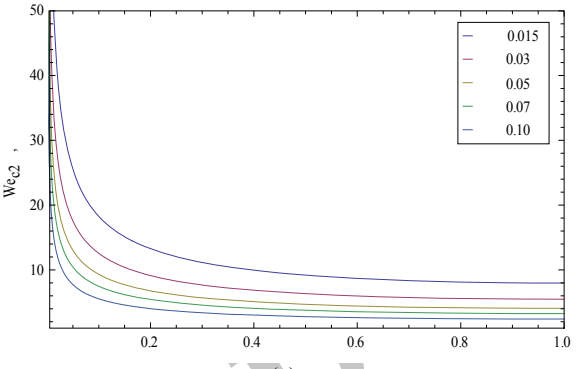

(a)

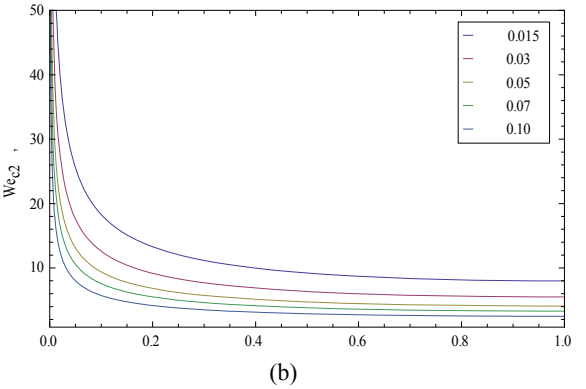

(b)

Fig. 3 Marginal stability curves for $\epsilon \in [0.015,0.10]$ for the second critical weisenberg number We_{C2}. The curves are plotted against ζ for the range [0,1]. Note that curves are symmetric with respect to $\zeta = 1$. The approximate curves based on the six-dimensional model system (B1) are shown in (a), and the exact curves are shown in (b)

Table 1 Comparison between exact and approximate critical Weissenberg numbers for $\zeta \in [0,1]$and$\epsilon = 0.05$. The six-dimensional model is used in this comparison.

	Approximate		Exact	
ζ	We_{c1}	We_{c2}	We_{c1}	We_{c2}
0.1	2.717	9.318	2.569	9.388
0.3	1.658	5.687	1.568	5.730
0.5	1.367	4.690	1.293	4.725
0.7	1.242	4.258	1.174	4.290
0.9	1.190	4.082	1.125	4.113

The approximate values tend to be slightly lower. Figures 2(a) and 2(b) show that We_{c1} decreases monotonically as ζ increases. Note that the curves are symmetric with respect to $\zeta = 1$. Similar observations can also bemade regarding the marginal stability curves for the secondcritical Weissenberg number as depicted from Fig. 3. In thiscase, the approximate value for We_{c2} tends to be higher than the exact value. A sample

of the two critical Weissenberg numbers are shown in Table 1, where the quantitative agreement between the exact and approximate values for $We_{c1}$and We_{c2} is clearly illustrated.

The agreement in Figs. 2 and 3, and Table 1, between the approximate and exact marginal stability curves therefore justifies the current choice of the nature and number of eigenmodes and truncation level in the linear range.

3.2. Bifurcation and steady-state solution branches

The steady-state solutions of system (B1) are obtained upon setting the time derivatives to zero. A trivial solution exists when all the variables are zero. The other nontrivial solutions, however, can be generally obtained using a modified Newton–Raphson method. However, due to the nonlinearities involved, it is found that it is difficult to generate the steady-state branches for various values of We and ζ (recallthat Re influences only the transient solution). This difficultyis overcome by transforming the algebraic equations into aset of ordinary differential equations, governing the steady-
statevalues
$N_1^s(We,\zeta), N_2^s(We,\zeta), S_1^s(We,\zeta), S_2^s(We,\zeta), u_1^s(We,\zeta)$ and $u_2^s(We,\zeta)$, with We being the independent variable. Thus, if system (B1) is rewritten leading to Eq. (25).

$$\frac{dx}{dt} = F(x;We), \tag{25}$$

then the steady-state solution is obtained from $F(x;We) = 0$. This is a set of nonlinear algebraic equations that areconverted into a set of nonautonomous ordinary differential equations of the form of Eq. (26).

$$\frac{dx}{d\,We} = G(x;We). \tag{26}$$

Thus, a solution branch is sought for a given ζ and ε byseeking one solution point using the Newton–Raphson method. Bytaking this solution point as an initial condition, the solution branch is generated using a sixth-order Runge–Kutta algorithm. Note that an initial point on a stable solution branch can also be generated from the time-dependent solution of system (B1), without having to use the Newton–Raphson method. This route turned out to be quite effective and easily allows the generation of a high number of points along a solution branch. The first set of steady-state solution branches found turned out to be stable.

They are shown in Figs. 2-7. Each of the steady-state variables $N_1^s(We,\zeta), N_2^s(We,\zeta), S_1^s(We,\zeta), S_2^s(We,\zeta), u_1^s(We,\zeta)$ and $u_2^s(We,\zeta)$ are plotted against We for the range $\zeta \in [0,1]$ and $\varepsilon = 0.04$. It is apparent from Figs. 2-7 that the origin in phase space (base flow) remains the only steady-state solution of system (B1) for $We < We_{c1}$and $We > We_{c2}$.

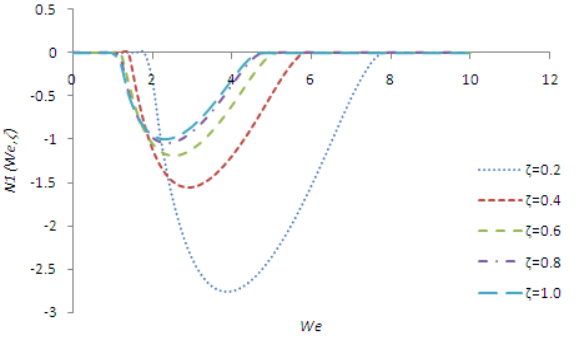

Fig. 4 Stable steady-state solution branches $N_1^s(We,\zeta)$ as function of We for $\zeta \in [0,1]$ and $\varepsilon = 0.04$

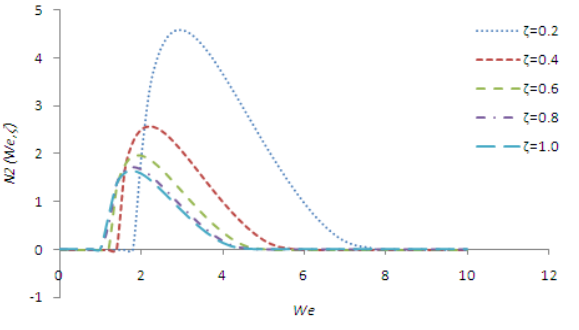

Fig. 5 Stable steady-state solution branches $N_2^s(We,\zeta)$ as function of We for $\zeta \in [0,1]$and $\varepsilon = 0.04$. Note that the branches are symmetric with respect to the horizontal axis

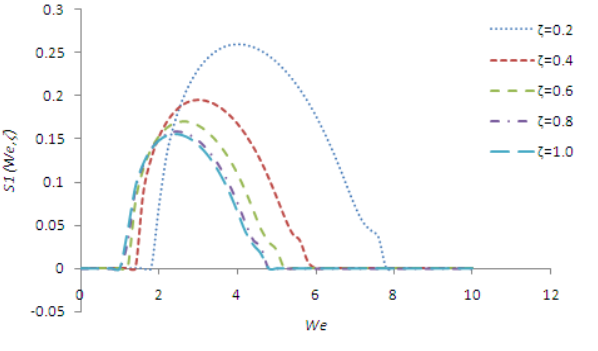

Fig. 6 Stable steady-state solution branches $S_1^s(We,\zeta)$ as function of We for $\zeta \in [0,1]$and $\varepsilon = 0.04$. Note that the branches are symmetric with respect to the horizontal axis

For the range $We_{c1} < We < We_{c2}$, an additional fixed branch emerges, which coincides with the loss of stability of the base flow and the emergence of a stable nonlinear velocity profile. The nature of the bifurcation at the two critical points remains to be established from linear stability analysis. From the structure of system

(B1), it is not difficult to see that the three sets of solution branches corresponding to $N_2^s(We,\zeta)$, $S_1^s(We,\zeta)$ and $u_1^s(We,\zeta)$ in Figs. 3, 4 and 6, respectively, are symmetric with respect to the zero (horizontal) axis.

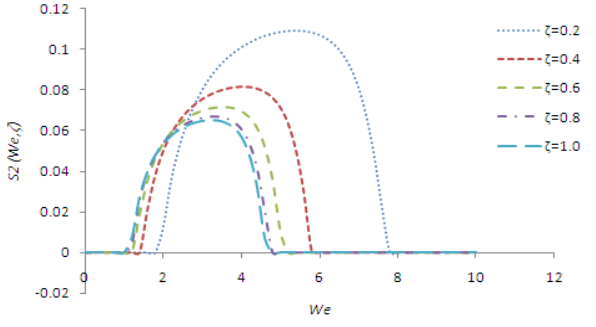

Fig. 7 Stable steady-state solution branches $S_2^s(We,\zeta)$ as function of We for $\zeta \in [0,1]$ and $\varepsilon = 0.04$

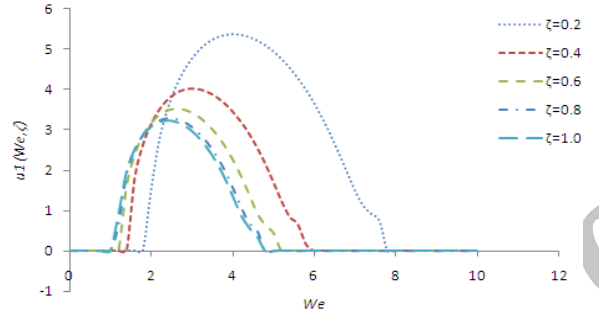

Fig. 8 Stable steady-state solution branches $u_1^s(We,\zeta)$ as function of We for $\zeta \in [0,1]$and $\varepsilon = 0.04$. Note that the branches are symmetric with respect to the horizontal axis

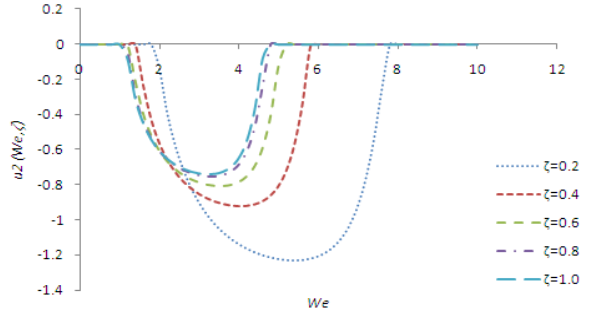

Fig. 9 Stable steady-state solution branches $u_2^s(We,\zeta)$ as function of We for $\zeta \in [0,1]$ and $\varepsilon = 0.04$

4 TRANSIENT BEHAVIOR AND NONLINEAR DYNAMICS

Although linear stability analysis or center-manifold theory allows the determination of conditions for instability of the steady-state branches, only behavior in the vicinity of these branches can be predicted. The full range of dynamical behavior can only be understood when the numerical solution of the nonlinear system (B1) is obtained. The time-dependent evolution of flow is examined using a sixth-order Runge–Kutta scheme[13]. Obviously, the solution depends on the initial conditions assumed. However, regardless of these conditions, the long-term behavior will be essentially the same, after transients have died out; it is this behavior that is of interest here. Before examining nonlinear behavior as a flow approaches the steady state (base flow or other nontrivial state), it is useful to first examine the influence of Re.

4.1. Nonlinear and transient behavior

Nonlinear behavior is now explored by examining the time-dependent solution as the flow is perturbed initially from rest. Many cases were studied in an attempt to understand the role of acceleration and elasticity. Typically, for a given case, We is usually kept fixed andRe is varied. All three ranges,$We < We_{c1}$, $We_{c1} < We < We_{c2}$and $We > We_{c2}$, were explored. Aside from the difference in the (final) steady-state solution, the transient behavior is found to be monotonic for $Re < Re_0$ and oscillatory for $Re > Re_0$where Re_0 is given by characteristic equations that have emerged from linearizing system (B1) around the base flow. For this reason, only some of the typical results will be presented next. The discussion is also restricted to$\varepsilon = 0.04$and$\zeta = 0.2$. In this case,$We_{c1} = 1.92$ and $We_{c2} = 7.74$. To enhance the dynamical behavior, the initial conditions are taken to correspond to large values of the flow variables, in comparison with the steady-state solution. Thus, the following conditions are assumed: $u_1(0) = u_2(0) = N_1(0) = N_2(0) = S_1(0) = S_2(0) = 1$. The resulting dynamicsis depicted in Figs. 8-10 for various values of the Weissenberg numbers. The evolution of the (total) velocity, shear stress and normal stress difference profile between the two plates is shown in Figs. 8(a) , 8(b) and 8(c) respectively. These cases will allow some comparison with the finite-element results of Georgiou and Vlassopoulos[14].

A direct comparison on a case-by-case basis is difficult to make given the multiplicity of flow for a given set of parameters. It is reported in Ref. [14] that the finite-element method gives a different (steady-state) flow when the mesh size is changed. So, even if the initial conditions are taken to correspond to those of Georgiou and Vlassopoulos [14], it is extremely difficult to fine-tune the numerical integration to obtain the same steady-state profile. However, comparison becomes easier to conduct with only steady-state profiles. Consider first the behavior of the flow for a precritical value for the Weissenberg number($We < We_{c1}$), namely, $We = 1$. The Reynolds number is fixed at

$Re = 0.1$. In thiscase, the base flow is unconditionally stable, and the solutionevolves toward the origin. For $We = 1, Re_0 = 0.0065$. One thus expects an oscillatory approach to the base flow. Indeed, Fig. 8 indicates that the flow does not converge monotonically towards the Couette(base) flow. There is in fact an oscillatory behavior about the origin (base flow). The flow tends to grow in amplitude at the early stages, exceeding the initial amplitude. The wave number is approximately equal to 1.77, and steady-state conditions are attained at approximately= 3 We. The behavior in Fig. 8 is comparable to that reported in Figs. 9 and 10 of Ref. [14].

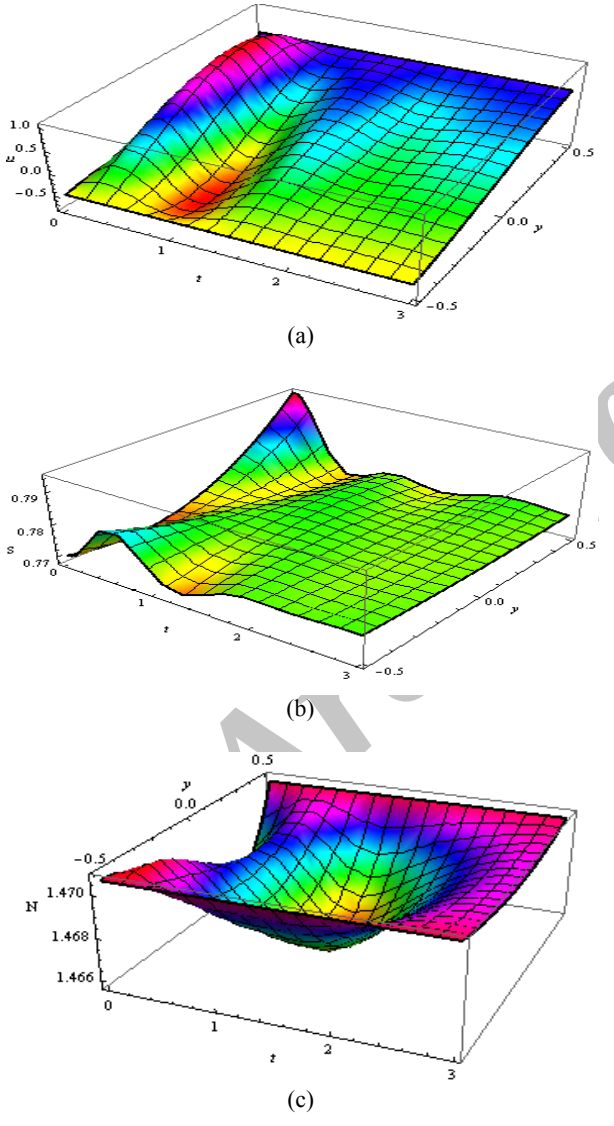

Fig. 10 Transient behavior of flow in the precriticalrange ($We < We_{c1}$). Evolution of solution towards the base flow for $Re = 0.1, We = 1, \varepsilon = 0.04$ and $\zeta = 0.2$. In this case, since $Re > Re_0 = 0.0065$, the behavior is oscillatory. Evolution of velocity (a), shear stress (b) and normal stress difference (c) are shown

Although the initial conditions in the two situations are not the same, both results show an oscillatory behavior around the base flow, and comparable times for steady-state conditions to set in. Georgiou and Vlassopoulos have reported the time as 2.25 (Fig. 10 in Ref. [14]). Nevertheless, the present results indicate that the frequency generally increases with the Weissenberg number, an observation that is also in agreement with Ref. [14]. Thus, if two fluids with similar properties are considered, the fluid with a larger viscosityrelaxes faster. For the case of design of viscoelastic damper the no dimensional force on plates are calculated for different damping agent and is shown in Fig. 11. Note that transient force increases with the viscoelasticity effect ζ. All solutions reach steady-state solution in almost 2 nondimensional time units.

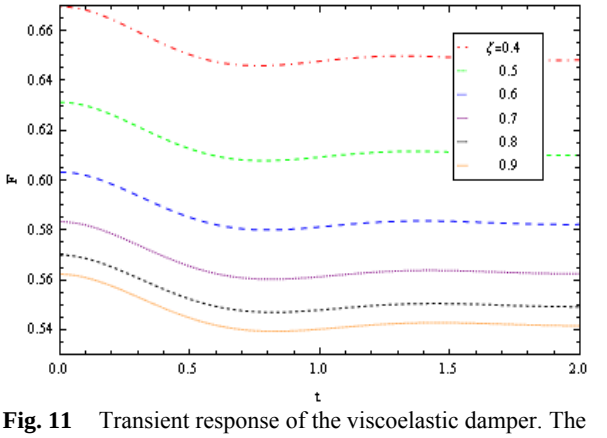

Fig. 11 Transient response of the viscoelastic damper. The transient force on the plates is shown for $We = 1$, $Re = 0.1$, $\zeta \in [0.4,0.9]$ and $\varepsilon = 0.04$

5 CONCLUSION

The applicability of low-order dynamical systems is explored for the channel flow of viscoelastic fluids. The linearand the nonlinear stabilities of viscoelastic plane Couette flow are examined for a Johnson–Segalman fluid with added Newtonian viscosity. This is one of the very few constitutive models that gives rise to linearly unstable flow for the range of Weissenberg numbers that correspond to a negative slope in the shear-stress/shear-rate curve. Given the complexity of the constitutive equation and the potentially intricate interplay between fluid inertia and elasticity, only 1-D disturbances are considered here.

Four dimensionless groups emerge in the formulation, namely, the Reynolds number,Re, the Weissenberg number, We, the solvent-to-solute viscosity ratio, ϵ, and the slip parameter, ζ, in the constitutive model. In the present problem, nonlinearities are confined to the convective, upper- and lower-convective terms in the constitutive equation. A dynamical system approach

based on the Galerkin projection method is adopted to describe the flow as Re and $We$is varied. The nonlinear dynamical system is derived by expanding the flow field (velocity and stress) into odd and even Chandrasekhar functions along the direction perpendicular to the flow. A suitable truncation level is adopted to close the hierarchy of the resulting set of ordinary differential equations. Although the formulation accommodates an arbitrary number of modes, it is found that a six-dimensional dynamical system is sufficient for a reasonably accurate qualitative description of flow behavior.

For given ζ and ε, two critical values of the Weissenbergnumber, We_{c1} and We_{c2} ($We_{c1} < We_{c2}$) are found, atwhich an exchange of stability takes place between the baseflow and a nontrivial steady-state branch (nonlinear velocityprofile). These critical Weissenberg numbers are in close agreement with the ones found analytically. The two critical points coincide with the extrema of the shear-stress/shearrate curve. There are thus three ranges of Weissenberg numbers of interest that are investigated, namely, the precriticalrange $We < We_{c1}$, the critical range, $We_{c1} < We < We_{c2}$, and the postcritical range, $We > We_{c2}$. Since thetwo critical points are nonhyperbolic fixed points, linear stabilityanalysis cannot be used to determine the stability nearthese points.

Although the Reynolds number does not influence the value of the critical Weissenberg numbers,$We_{c1}$and We_{c2},or the bifurcation picture, it has a significant influence on thetransient behavior. Linear stability analysis about the baseflow (origin in phase space) shows that, at low Reynolds number, the base flow is approached monotonically with time. AsRe exceeds a critical value,$Re_0(We, \varepsilon, \zeta)$, oscillatorybehavior sets in during the transient flow.

A similar influence ofRe is also experienced by the flow as it approaches a non-trivial steady state. Various scenarios are explored to understand transient and nonlinear behavior by varying Re and We. Results are depicted in Figs. 8, where the flow in the precritical, critical, and postcriticalranges ofWe are investigated. It is generally found that the time a flow takes to reach steady state increases as the Reynolds number increases. Thus, the more viscous fluids, for a given level of elasticity, tend to relax faster.

Finally, the issue of the low-order representation of the flow field remains an unsettled question, in general and especially in the present context. The method of Galerkin projection with the use of orthonormal functions is essentially alinear concept that has seen its validity extended to then online arrange, and has given rise to modern and powerful techniques for the solution of complex partial differential equations such as the spectral or pseudo spectral methods. Fundamentally speaking, an in finite number of modes are needed to represent accurately the discontinuity. From a more pragmatic point of view, however, one may counter-argue that if the discontinuous profiles are reasonably approximated by the low-order approximation, then the low-order approximation is reasonably adequate. One should then view the present approach, the governing equations as well as their approximate solution, as a simple theoretical modelling tool that has yet to prove its validity once direct comparison with experiment becomes possible.

REFERENCES

[1] Sell, G. R., Foias, C., and Temam, R., "Turbulence in Fluid Flows: A Dynamical Systems Approach", Springer, New York, 1993.

[2] Holmes, P., Lumley, J. L., and Berkooz, G., "Turbulence, Coherent Structures, Dynamical Systems and Symmetry", Cambridge University Press, Cambridge, 1996.

[3] Lorenz, E. N., "Deterministic nonperiodic flow", J. Atmos. Sci., Vol. 20, 1963, pp. 130-141.

[4] Shirer, H. N., and Wells, R., "Mathematical Structure of the Singularities at the Transition Between Steady States in Hydrodynamic Systems", Springer, Heidelberg, 1980.

[5] Veronis, G., "Motions at subcritical values of the rayleigh number in a rotating fluid", J. Fluid Mech. Vol. 24, 1966, pp. 545-554.

[6] McLaughlin, J. B., and Martin, P. C., "Transition to urbulence in a statically stressed fluid system", Phys. Rev. A 12, 1975, pp. 186-2031975.

[7] Curry, J. H., "A generalized lorenz system", Commun. Math. Phys. Vol. 60, No. 3, 1978, pp. 193-204.

[8] Khayat, R. E., "Low-dimensional approach to nonlinear overstability of purely elastic Taylor-vortex flow", Phys. Rev. Lett. Vol. 78, No. 26, 1997, pp. 4918-4921.

[9] Singh, M. P., and Chang, T. S.,"Seismic analysis of structures with viscoelastic dampers", J. Eng. Mech., Vol. 135, No. 6, 2009, pp. 571-580.

[10] Bird, R. B.,Armstrong, R. C., and Hassager, O., "Dynamics of Polymeric Liquids", 2nd Ed. Wiley, New York, Vol. 1, 1987.

[11] Chandrasekhar, S., "Hydrodynamic and Hydromagnetic Stability", Dover, New York, 1961.

[12] Ashrafi, N., and Khayat,R. E., "A low-dimensional approach to nonlinear plane-Couette flow of viscoelastic fluids", Vol. 12, No. 2, 2000, pp. 345-366.

[13] Hansen, S., "Estimation of the relaxation spectrum from dynamic experiments using Bayesian analysis and a new regularization constraint", Rheol Acta, Vol. 47, No. 2, 2007, pp. 169-78.

[14] Georgiou, G. C., and Vlassopoulos, D., "On the stability of the simple shear flow of a Johnson–segalman fluid", J. Non-Newtonian Fluid Mech., Vol. 75, No. 1, 1998, pp. 77-79.